DOI 10.15622/ia.2020.19.5.2

T. ENDO , R. MAEDA , F. MATSUNO

STABILITY ANALYSIS OF SWARM HETEROGENEOUS ROBOTS WITH LIMITED FIELD OF VIEW

Endo T., Maeda R., Matsuno F. **Stability Analysis of Swarm Heterogeneous Robots with Limited Field of View.**

Abstract. This paper presents a stability analysis of swarm robots, a group of multiple robots. In particular, we focus on robot swarms with heterogeneous abilities, in which each robot has a different sensing range and physical limitations, including maximum velocity and acceleration. In addition, each robot has a unique sensing region with a limited angle field of view. We previously proposed a decentralized navigation method for such heterogeneous swarm robots consisting of one leader and multiple followers. With the decentralized navigation method, a single leader can navigate for followers while maintaining connectivity and satisfying the physical limitations unique to each robot; i.e., each follower has a target robot and follows it without violating its physical limitations. In this paper, we focus on a stability analysis of such swarm robots. When the leader moves at a constant velocity, we mathematically prove that the shape and orientations of all robots eventually converge to the equilibrium state. For this, we must first prove that the equilibrium state exists. Then, we show the convergence of the state to its equilibrium. Finally, we carry out experiments and numerical simulations to confirm the stability analysis, i.e., the convergence of the swarm robots to the equilibrium states.

Keywords: stability, swarm robots, navigation, decentralized controller

1. Introduction. Swarm robots are a group of multiple robots that aim to achieve robust, scalable, and flexible coordinated collective behavior [1-6]. For robot swarms, it is important to control the robots in a decentralized manner by utilizing locally available information for each robot, so that the system can deal with increases in the number of robots. Swarm robots are expected to be applicable to various situations, such as cooperative coverage [7, 8], surveillance [9, 10], target-capturing [11, 12], transport [13, 14], and visually appealing entertainment [15, 16]. One of the essential functions of such tasks is to move swarm robots as a flock to the desired location.

Although many studies have investigated the connectivity maintenance of swarm robots, most have considered homogeneous swarm robots, which consist of robots with the same ability and performance. On the other hand, heterogeneous swarms consist of robots with different abilities and performance. Heterogeneous swarm robots have the ability to handle a wide range of tasks that homogeneous swarms cannot. This is because they cooperate with each other while taking advantage of each robot's characteristics [17]. For example, several studies [18-20] proposed decentralized control methods for connectivity maintenance of a group of heterogeneous robots characterized by a different communication radius. Another study [21] also proposed a decentralized control method for connectivity maintenance of a robotic swarm

with heterogeneous abilities, including sensing range, maximum velocity, and acceleration. However, these studies assumed that all robots could sense all directions.

In practical situations, many sensors and cameras have angle limitations in addition to distance ones in the sensing range. Thus, to propose a decentralized control method for connectivity maintenance of a heterogeneous robotic swarm, in which each robot has both a different sensing range with a limited field of view and a limited sensing distance, is a practical challenge. A few studies [22-26] have considered the navigation of robots having cameras with a limited field of view. In three [22-24], control methods were proposed for visibility maintenance of homogeneous robots; i.e., each robot had the same sensing region, and a cooperative visibility maintenance method was proposed in [25] for multiple robots with different sensing regions but the same performance.

However, there are no studies about decentralized control methods for connectivity maintenance of a heterogeneous robotic swarm characterized by sensing distance, limited field of view, and maximum velocity and acceleration. We previously proposed a decentralized navigation strategy for swarm robots with heterogeneous abilities, including the angle of field of view, velocity, and acceleration [26]. Our method ensured that the leader could guide the followers. At the same time, they maintained a certain distance from their target and did not exceed their unique physical limitations such as maximum velocity and acceleration. However, we did not conduct a stability analysis of swarm robots.

In this paper, we present the stability analysis of swarm robots with heterogeneous abilities for velocity and acceleration, and sensing region with a limited angle of view, and limited sensing distance. We discuss the stability of the whole swarm shape, and the orientation of each follower robot with omni-directional mobility; i.e., we discuss the convergence of the shape of the whole swarm and the orientation of all followers to the equilibrium state. The stability of the swarm shape predicts the shape of the swarm, which is useful in controlling formation or avoiding obstacles. On the other hand, the stability of followers' orientation greatly influences on their ability to keep the target robot in their sensing range, which is important in connectivity maintenance with robots having a limited field of view. Thus, we prove that the swarm shape and the orientation of all followers converge to an equilibrium state. Further, we present experimental results and numerical simulation results to confirm the validity of our stability analysis. The preliminary version of this paper has been published [27]. This extended version contains a new proof of the boundedness of perturbation, that is required in the stability of the whole

swarm. Furthermore, this paper includes new simulation results to investigate the stability of the swarm robots by our control method for a more significant number of robots.

The main contributions of this paper are as follows. We deal with a heterogeneous swarm of robots in which each robot has a different sensing range, limited field of view, and physical limitations, such as maximum velocity and acceleration. Such robotic swarms have the potential to deal with a wider variety of tasks. When a leader robot guiding follower robots moves at a constant speed in a constant direction, the shape of the whole swarm and all followers' orientations converge to an equilibrium point. We mathematically prove that this convergence is achieved, and carry out an experiment and numerical simulation to confirm the stability.

This paper is organized as follows. In Section 2, we present the problem settings. Section 3 introduces our navigation method. Section 4 describes the mathematical analysis of stability. Section 5 provides the experimental results and Section 6 the results of the numerical simulations to confirm the stability analysis. Finally, Section 7 concludes the paper.

2. System Description. Let us consider $n+1$ agents in a two-dimensional (2-D) plane without obstacles. ID $1,2,\ldots,n$ are assigned to followers, and $n+1$ to the leader. The position vector and orientation of agent i in the absolute coordinate system at time t are $\boldsymbol{x}_i(t) = [x_i(t), y_i(t)]^T \in \mathbb{R}^2$ and $\eta_i(t) \in \mathbb{R}$, respectively, and the equations of motion of agent i are described as follows:

$$\dot{\boldsymbol{x}}_i(t) = \boldsymbol{u}_i(t); \tag{1}$$

$$\dot{\eta}_i(t) = \omega_i(t), \tag{2}$$

where $\boldsymbol{u}_i(t) \in \mathbb{R}^2$ is translational velocity input, and $\omega_i(t) \in \mathbb{R}$ is angular velocity input. Follower i has the following physical limitations:

$$\begin{cases} \|\boldsymbol{u}_i(t)\| \leqslant U_i, \quad \|\dot{\boldsymbol{u}}_i(t)\| \leqslant A_i, \quad |\omega_i(t)| \leqslant \Omega_i, \quad |\dot{\omega}_i(t)| \leqslant B_i; \\ \boldsymbol{u}_i(t) \text{ and } \omega_i(t) \text{ are continuous for } t, \end{cases} \tag{3}$$

where $\dot{\boldsymbol{u}}_i(t)$ is the semi-derivative of $\boldsymbol{u}_i(t)$, whose norm is larger if $\boldsymbol{u}_i(t)$ is left or right semi-differentiable, and $\dot{\omega}_i(t)$ is defined in the same manner. In addition, U_i, A_i, Ω_i, and B_i are the upper limits of the translational velocity, translational acceleration, angular velocity, and angular acceleration, respectively, and $\|\cdot\|$ denotes the Euclidean norm.

The sensing region of follower i is defined as follows:

$$S_i(t) = \left\{ \boldsymbol{x}(t) \in \mathbb{R}^2 \ : \ r_i(t) \leqslant \rho_i, \ |\phi_i(t)| \leqslant \psi_i \right\}, \tag{4}$$

where $\boldsymbol{x}(t) = [x(t), y(t)]^T \in \mathbb{R}^2$ is a position vector, $r_i(t) = \|\boldsymbol{x}(t) - \boldsymbol{x}_i(t)\| \in \mathbb{R}$ is the distance between $\boldsymbol{x}(t)$ and follower i, ρ_i is the maximum sensing distance, $\phi_i(t)$ is the bearing angle from follower i to $\boldsymbol{x}(t)$, which is defined by $\phi_i(t) = \text{atan2}(y(t) - y_i(t), \ x(t) - x_i(t)) - \eta_i(t)$, and $2\psi_i(t)$ is the angle of the sensing region as shown in Figure 1 (a). If agent j is in the sensing region $S_i(t)$, follower i can measure the relative distance $r_{ij}(t) = \|\boldsymbol{x}_j(t) - \boldsymbol{x}_i(t)\|$ and bearing angle $\phi_{ij}(t) = \text{atan2}(y_j(t) - y_i(t), \ x_j(t) - x_i(t)) - \eta_i(t)$.

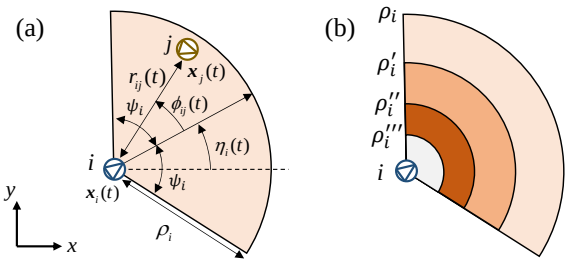

Fig. 1. Sensing region of follower i: (a) relative position between follower i and its target; (b) division of sensing region

We assume that the leader knows the specifications of all followers, but cannot access global real-time information. Meanwhile, followers can obtain only local information from their own sensing.

3. Previously Proposed Navigation Method. In this section, we briefly introduce our previously proposed decentralized navigation method [26] for heterogeneous swarm robots with a limited field of view, which ensures connectivity maintenance.

The translational velocity input of follower i is set as the following form:

$$\boldsymbol{u}_i(t) = u_{ir}(t)\boldsymbol{e}_{ir}(t) + u_{i\theta}(t)\boldsymbol{e}_{i\theta}(t), \tag{5}$$

where the target of follower i is agent j, $\boldsymbol{e}_{ir}(t)$ is a unit vector defined by $\boldsymbol{e}_{ir}(t) = (\boldsymbol{x}_j(t) - \boldsymbol{x}_i(t))/r_{ij}$, and $\boldsymbol{e}_{i\theta}(t)$ is a unit normal vector of $\boldsymbol{e}_{ir}(t)$ (see Figure 2 (a)). We define positive constants ρ_i', ρ_i'', and ρ_i''', which satisfy $0 < \rho_i''' < \rho_i'' < \rho_i' < \rho_i$, respectively, and divide the sensing region as shown in Figure 1 (b). Then, the components of $\boldsymbol{u}_i(t)$ are designed as follows:

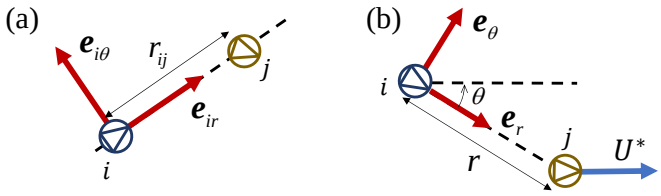

Fig. 2. Relationship between follower i and its target j: (a) local coordinate system; (b) definition of angle θ

1. If $\rho_i''' \leqslant r_{ij}(t) \leqslant \rho_i''$;

$$\begin{cases} u_{ir}(t) = a_i'(r_{ij}(t) - \rho_i''), \\ u_{i\theta}(t) = 0. \end{cases} \tag{6}$$

2. If $\rho_i'' < r_{ij}(t) < \rho_i'$;

$$\begin{cases} u_{ir}(t) = 0, \\ u_{i\theta}(t) = 0. \end{cases} \tag{7}$$

3. If $\rho_i' \leqslant r_{ij}(t) < \rho_i' + \frac{U_i'(t)}{2a_i}$;

$$\begin{cases} u_{ir}(t) = a_i(r_{ij}(t) - \rho_i'), \\ u_{i\theta}(t) = \sigma_i u_{ir}(t). \end{cases} \tag{8}$$

4. If $\rho_i' + \frac{U_i'(t)}{2a_i} \leqslant r_{ij}(t) \leqslant \rho_i' + \frac{U_i'(t)}{a_i}$;

$$\begin{cases} u_{ir}(t) = a_i(r_{ij}(t) - \rho_i'), \\ u_{i\theta}(t) = \sigma_i(U_i'(t) - u_{ir}(t)). \end{cases} \tag{9}$$

Here, $a_i = U_i/(\rho_i - \rho_i')$, $a_i' = V_i(\rho_i'' - \rho_i''')$, $\sigma_i(t) \in [-1, 1]$, V_i is a parameter satisfying $V_i \leqslant U_i$ (the definition is described in [26]), and $U_i'(t) = \max_{0 \leqslant \tau \leqslant t} u_{ir}(\tau)$. By this control method, the relations

$$\rho_i''' \leqslant \rho_i'' - \frac{U_{n+1}}{a_i'} < r_{ij}(t) \leqslant \rho_i' + \frac{U_i'(t)}{a_i} \tag{10}$$

always hold [26], and thus it is enough to design the translational velocity input in the above range. In addition, the parameter $\sigma_i(t)$ affects the shape of the swarm. The larger $|\sigma_i(t)|$, the wider the swarm shape becomes. The control input (6) moves the follower away from its target when they are too close. By (8) and (9), the follower maintains connectivity with its target while satisfying translational limitations (first and second limitations in (3)).

On the other hand, angular velocity input $\omega_i(t)$ is given by

$$\omega_i(t) = k_i \phi_{ij}(t). \tag{11}$$

Here, the feedback gain k_i satisfies

$$\frac{K_i}{\psi_i} \leqslant k_i \leqslant \min\left\{ \frac{\Omega_i}{\psi_i}, \frac{-K_i + \sqrt{K_i^2 + 4\psi_i B_i}}{2\psi_i} \right\}, \tag{12}$$

where $K_i = \max\{V_i/\rho_i''', 3a_iV_i/(2a_i\rho_i' + V_i)\}$. By the control input (11), the follower turns to its target while satisfying rotational limitations (third and fourth limitations in (3)).

When the followers are controlled by (5)–(9) and (11), connectivity maintenance of the whole swarm is achieved by introducing some proper velocity constraints for the leader. Details of leader constraints, the definition of connectivity, the target determination method, and proof of satisfying physical limitations and connectivity maintenance are described in our previous paper [26].

Here, note that we did not consider the case of failure of the leader robot. Robustness against failure is an important issue we leave for future study.

4. Stability Analysis. We show that the shape of the whole swarm and orientation of all followers converge to the equilibrium state when the leader moves at a constant velocity. Since in Sections 4.1 and 4.2 we mainly consider two agents, i and its target j, we hereafter omit the subscripts i and ij for parameters and variables. In addition, let us define the following:

$$r_c := \rho' + \frac{U'}{2a}, \quad r_e := \rho' + \frac{U'}{a}, \quad r_d := \rho'' - \frac{U_{n+1}}{a'}. \tag{13}$$

We assume that agent j moves at constant velocity $\|\boldsymbol{u}_j\| = U^*$, and thus we also assume that σ is a constant. Here, we consider only the case of $\sigma \geqslant 0$, because $\sigma \geqslant 0$ and $\sigma \leqslant 0$ are physically symmetric from the definition of $u_{i\theta}$. By defining θ as the angle between $\boldsymbol{e}_r$ and the moving direction of agent j as

shown in Figure 2 (b), the kinematic model of this motion is given by

$$\dot{r} = U^* \cos\theta - u_{ir}, \tag{14}$$

$$\dot{\theta} = \frac{1}{r}(u_{i\theta} - U^* \sin\theta), \tag{15}$$

$$\dot{\phi} = \frac{1}{r}(U^* \sin\theta - u_{i\theta}) - k\phi = -\dot{\theta} - k\phi. \tag{16}$$

First, we define the equilibrium point.

Definition 1. (Equilibrium point): The equilibrium for a parameter U^* is a point (r_0, θ_0, ϕ_0) that satisfies $\dot{r}|_{r=r_0} = 0$, $\dot{\theta}\big|_{\theta=\theta_0} = 0$, and $\dot{\phi}\big|_{\phi=\phi_0} = 0$, for fixed $U^* \in (0, U']$.

We prove an equilibrium exists for $U^* \in (0, U']$. On the other hand, from (14)–(16), r and θ are independent of ϕ. Therefore, we discuss the convergence of relative position (r, θ) first, and then that of bearing angle ϕ in the following subsection. We hereafter consider θ in $(-\pi, \pi]$.

4.1. Equilibrium point of relative position.

Lemma, 1. (Existence of the equilibrium): Let us consider the system (14) *and* (15). *For $U^* \in (0, U']$, one stable equilibrium point exists in an area $\rho' < r \leqslant r_e$ and $0 \leqslant \theta \leqslant \tan^{-1}\sigma$. Moreover, there is one saddle point in an area $r_d \leqslant r < \rho''$. The equilibrium point (r_0, θ_0) is continuous for U^*, and r_0 is monotonically increasing for U^* if $r > \rho'$, and monotonically decreasing if $r < \rho''$.*

Proof. We divide the proof into two steps:

(step 1): We show the existence of the equilibrium.

1) If $r_d \leqslant r < \rho''$, from (6), (14), (15), and Definition 1, (r_0, θ_0) should satisfy $U^* \cos\theta_0 - a'(r_0 - \rho'') = 0$ and $U^* \sin\theta_0 / r_0 = 0$. Then, we obtain $(r_0, \theta_0) = (\rho'' - U^*/a', \pi)$. We call this point P and define $r_p := \rho'' - U^*/a'$. Point P is obviously continuous and monotonically decreasing for U^*.

2) If $\rho'' \leqslant r \leqslant \rho'$, from (7), (14), and (15), (r_0, θ_0) should satisfy $U^* \cos\theta_0 = 0$ and $-U^* \sin\theta_0 / r_0 = 0$. However, there is no (r_0, θ_0) satisfying these equations simultaneously because of $U^* > 0$.

3) If $\rho' < r < r_c$, from (8), (14), and (15), the equilibrium satisfies

$$\begin{cases} U^* \cos\theta_0 - a(r_0 - \rho') = 0, \\ \sigma a(r_0 - \rho') - U^* \sin\theta_0 = 0. \end{cases} \tag{17}$$

Since $U^* > 0$ and $r_0 > \rho'$, $\sin\theta_0 \geqslant 0$ and $\cos\theta_0 \geqslant 0$ must hold. Then $0 \leqslant \theta_0 \leqslant \pi/2$. From (17), we obtain $\sin\theta_0 - \sigma\cos\theta_0 = 0$ and $\theta_0 = \tan^{-1}\sigma$. Considering $0 \leqslant \theta_0 \leqslant \pi/2$ gives $\cos\theta_0 = 1/\sqrt{1+\sigma^2}$, substituting this into

the first equation in (17), we obtain $(r_0, \theta_0) = (\rho' + U^*/(\sqrt{1+\sigma^2}a), \tan^{-1}\sigma)$ for $U^* \in (0, \sqrt{1+\sigma^2}U'/2)$. This point is continuously in $\rho' < r < r_c$, and r_0 is monotonically increasing for U^*.

4) If $r_c \leqslant r \leqslant r_e$, the equilibrium point satisfies

$$\begin{cases} U^* \cos\theta_0 - a(r_0 - \rho') = 0, \\ a(U' - a(r_0 - \rho')) - U^* \sin\theta_0 = 0, \end{cases} \tag{18}$$

from (9), (14), and (15). Since $U^* > 0$ and $r_0 > \rho'$, $\sin\theta_0 \geqslant 0$ and $\cos\theta_0 > 0$ must hold, and these lead to $0 \leqslant \theta_0 < \pi/2$. From (18), we obtain

$$\sin\theta_0 + \sigma\cos\theta_0 = \frac{\sigma U'}{U^*}, \tag{19}$$

and a condition of existence of θ_0 is $U^* \geqslant \sigma U'/\sqrt{1+\sigma^2}$. Since $\sigma U'/\sqrt{1+\sigma^2} \leqslant \sqrt{1+\sigma^2}U'/2$ holds for any $\sigma \in [0,1]$ and $U' > 0$, the equilibrium point exists continuously in $r_c \leqslant r \leqslant r_e$ for $U^* \in [\sqrt{1+\sigma^2}U'/2, U']$. Since θ_0 ($\geqslant 0$) is monotonically decreasing for U^* from (19), and $\theta_0 = \tan^{-1}\sigma$ at $U^* = \sqrt{1+\sigma^2}U'/2$, we have $\theta_0 \leqslant \tan^{-1}\sigma$. Moreover, r_0 is monotonically increasing for U^*.

(step 2): Next, we discuss the stability of the equilibrium point.

1) If $r_d \leqslant r < \rho''$, from (14) and (15), Jacobi matrix J at equilibrium point P is calculated as follows:

$$J = \begin{bmatrix} \frac{\partial \dot{r}}{\partial r} & \frac{\partial \dot{r}}{\partial \theta} \\ \frac{\partial \dot{\theta}}{\partial r} & \frac{\partial \dot{\theta}}{\partial \theta} \end{bmatrix} = \begin{bmatrix} -a' & 0 \\ 0 & \frac{U^*}{r_0} \end{bmatrix}. \tag{20}$$

The eigenvalue of J is $\lambda = -a', U^*/r_0$, one of which is a negative real number, and the other a positive real number. Thus, P is a saddle point.

2) If $\rho' < r \leqslant r_e$, from (8) and (9), Jacobi matrix J at equilibrium point P is as follows:

$$J = \begin{bmatrix} -a & -U^* \sin\theta_0 \\ J_{21} & -\frac{U^*}{r_0}\cos\theta_0 \end{bmatrix}, \tag{21}$$

where $J_{21} = a\sigma/r_0$ when $\rho' < r_0 < r_c$, and $J_{21} = -a\sigma/r_0$ when $r_c \leqslant r_0 \leqslant r_e$. The characteristic equation of J is $\lambda^2 - (\mathrm{tr}J)\lambda + \det J = 0$, where λ is the

eigenvalue of J. Since $0 \leqslant \theta_0 \leqslant \tan^{-1}\sigma \leqslant \pi/4$ from lemma 1,

$$\mathrm{tr}J = -a - \frac{U^*}{r_0}\cos\theta_0 < 0 \tag{22}$$

$$\begin{aligned}\det J &= \frac{aU^*}{r_0}\cos\theta_0 \pm \frac{aU^*\sigma}{r_0}\sin\theta_0 \\ &\geqslant \frac{aU^*}{r_0}(\cos\theta_0 - \sigma\sin\theta_0) \geqslant 0\end{aligned} \tag{23}$$

are obtained. Here, note that $\det J = 0$ holds if and only if $\sigma = 1$, $U^* = U'/\sqrt{2}$, and $r_c \leqslant r_0 \leqslant r_e$. When $\det J \neq 0$, we have $\mathrm{Re}\lambda < 0$ from Hurwitz's theorem. Moreover, since

$$\begin{aligned}&(\mathrm{tr}J)^2 - 4\det J \\ &\quad = a^2 + \frac{U^{*2}}{r_0^2}\cos\theta_0 + \frac{aU^*}{r_0}(\cos\theta_0 - \sigma\sin\theta_0) > 0\end{aligned} \tag{24}$$

holds, λ is real and $\lambda < 0$.

Thus, the equilibrium is stable.

Next, let us consider the case of $\det J = 0$. In this case, the equilibrium is $(r_0, \theta_0) = (r_c, \pi/4)$, and one of the eigenvectors corresponding to $\lambda = 0$ is $[U^*/(\sqrt{2}a), -1]^T$. Since $\det J = 0$ does not hold in the direction of $r < r_c$, it is enough to consider the direction of the vector $[\Delta r, \Delta\theta]^T = \varepsilon[U^*/(\sqrt{2}a), -1]^T$ for $\varepsilon > 0$. Using a Taylor series in (14) and (15) around the equilibrium (r_0, θ_0), and substituting $[\Delta r, \Delta\theta]^T = \varepsilon[U^*/(\sqrt{2}a), -1]^T$ into them gives

$$\begin{aligned}\dot{r}(r_0 + \Delta r, \theta_0 + \Delta\theta) &= -a\Delta r - U^*\sin\theta_0\Delta\theta - \frac{U^*\cos\theta_0}{2}(\Delta\theta)^2 + \dots \\ &= -\frac{\varepsilon a}{2\sqrt{2}}\Delta r,\end{aligned} \tag{25}$$

$$\begin{aligned}\dot{\theta}(r_0 + \Delta r, \theta_0 + \Delta\theta) &= -\frac{\sigma a}{r_0}\Delta r - \frac{U^*\cos\theta_0}{r_0}\Delta\theta + \frac{\sigma a}{r_0^2}(\Delta r)^2 \\ &\quad + \frac{U^*\sin\theta_0}{2r_0}(\Delta\theta)^2 + \frac{U^*\cos\theta_0}{r_0^2}\Delta r\Delta\theta + \dots \\ &= -\frac{U^*\varepsilon}{2\sqrt{2}r_0}\Delta\theta.\end{aligned} \tag{26}$$

These show the equilibrium attracts points in the direction of $\varepsilon[U^*/(\sqrt{2}a), -1]^T$, and thus the equilibrium point (r_0, θ_0) is stable. □

Now, we discuss the convergence to the equilibrium point. First, we show the convergence of (r, θ), where $r \leqslant \rho'$.

Lemma, 2. (Convergence where $r \leqslant \rho'$): Let us consider the area $r \leqslant \rho'$. If $\theta = \pi$, (r, θ) converges to the saddle point P. If $\theta \neq \pi$, (r, θ) moves to the area $r > \rho'$ through $-\pi/2 \leqslant \theta \leqslant \pi/2$.

Proof. First, we consider the case in which the state converges to the saddle point P. Suppose $\theta(t') = \pi$ at the initial time t'. If $\rho'' < r(t') \leqslant \rho'$ and $\theta(t') = \pi$, we obtain $\dot{r} = -U^*$ and $\theta(t) = \pi$ from (7), (14), and (15). This means that r monotonically decreases until $r \leqslant \rho''$, while $\theta(t) = \pi$ is maintained. If r becomes $r \leqslant \rho''$, we obtain $\dot{r} = -U^* - a'(r - \rho'')$ and $\theta(t) = \pi$ from (6). Solving this equation under the initial condition $r(t_0) = \rho''$ gives $r(t) = \rho'' - U^*(1 - \exp(-a'(t - t_0)))/a' \to r_p$ as $t \to \infty$. Thus, (r, θ) converges to the saddle point P. The same discussion also holds if $r_d \leqslant r(t') \leqslant \rho''$.

Next, we consider the case in which $\theta \neq \pi$. Figure 3 shows the vector field where $r_d \leqslant r \leqslant \rho'$. Here, note that $r \geqslant r_d$ always holds as shown in [26]. The curved line in the area $r_p \leqslant r \leqslant \rho''$ shows $\theta = \cos^{-1}\{a'(r - r_p)/U^* - 1\}$, and $\dot{r} = 0$ holds on this line. Further, point (r, π) and $(r, -\pi)$ are the same point in the 2-D environment. Since the vector field is symmetrical concerning $\theta = 0$, we hereafter discuss the case where $\theta \geqslant 0$.

Let us divide the area $r \in [r_d, \rho']$ and $\theta \in [0, \pi)$ into the following four regions, as shown in Figure 3. The arrows in Figure 3 show the direction of velocity vector; that is, the possible region to which the state moves.

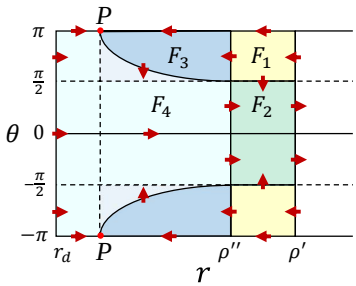

Fig. 3. Velocity field for $r \leqslant \rho'$

1) If (r, θ) is in the region F_1, $\theta = \pi$ will never hold, and the state moves to F_2 or F_3.

2) If (r, θ) is in the region F_2, $\theta < 0$ will never hold, and the state moves to the area $r > \rho'$.

3) If (r, θ) is in the region F_3, $\theta = \pi$ will never hold, and the state moves to F_4.

4) If (r,θ) is in the region F_4, $\theta=\pi$ and $\theta<0$ will never hold, and the state moves to F_2.

From these we find that (r,θ) always moves to the area $r>\rho'$ via the region F_2. Here, note that the same result is achieved in the case of $\theta\geqslant 0$ because of the symmetry of the vector field concerning to $\theta=0$. □

Note also that the convergence to the saddle point occurs only in limited situations, such as when the leader moves straight toward the follower whose target is the leader.

Next, we show the convergence of (r,θ) where $r>\rho'$. If the state starting from $r>\rho'$ becomes $(r,\theta)=(\rho',\pi)$, the state converges to the saddle point P from Lemma 2. Thus, we hereafter discuss the other case. First, we introduce the following theorems used in the proof.

Theorem, 1. (Poincaré-Bendixson Theorem [28]): Let $\boldsymbol{f}\in\mathbb{R}^2$ *be a* C^1 *function* $\mathbb{R}^2\to\mathbb{R}^2$. *If the equilibrium points of the differential equation* $\dot{\boldsymbol{x}}=\boldsymbol{f}(\boldsymbol{x})$ *are isolated, and the solution is bounded for* $t\geqslant 0$, *then either*

1. $\omega(\boldsymbol{x}(0))$ *is an equilibrium point, or*

2. $\omega(\boldsymbol{x}(0))$ *is a periodic orbit, or*

3. $\alpha(\boldsymbol{y})$ *and* $\omega(\boldsymbol{y})$ *are equilibrium points for each* $\boldsymbol{y}\in\omega(\boldsymbol{x}(0))$,

where $\alpha(\boldsymbol{x}(0))$ *and* $\omega(\boldsymbol{x}(0))$ *are an* α*-limit set and* ω*-limit set, respectively, of* $\dot{\boldsymbol{x}}=\boldsymbol{f}(\boldsymbol{x})$ *with the initial condition* $\boldsymbol{x}(0)$.

Since our system has non-C^1 input $u_{i\theta}$, we divide the whole region into the following four subregions to apply theorem 1 to our problem:

$$D_1=\left\{(r,\theta)\ :\ \rho'<r<\rho'+\frac{U^*}{a}\cos\theta,\ -\frac{\pi}{2}<\theta<\frac{\pi}{2}\right\}, \tag{27}$$

$$D_2=\begin{cases}\left\{(r,\theta)\ :\ \rho'<r<\min\left\{r_e,\rho'+\frac{U^*}{\sigma a}\sin\theta\right\},\ 0<\theta<\pi\right\} & \\ \qquad\qquad (0<\sigma\leqslant 1), & \\ \{(r,\theta)\ :\ \rho'<r<r_e,\ 0<\theta<\pi\} \qquad (\sigma=0), & \end{cases} \tag{28}$$

$$D_3=\begin{cases}\left\{(r,\theta)\ :\ \max\left\{\rho',r_e-\frac{U^*}{\sigma a}\sin\theta\right\}<r<r_e,\ 0<\theta<\pi\right\} & \\ \qquad\qquad (0<\sigma\leqslant 1), & \\ \{(r,\theta)\ :\ \rho'<r\leqslant r_e,\ 0<\theta<\pi\} \qquad (\sigma=0), & \end{cases} \tag{29}$$

$$D_4=\left\{(r,\theta)\ :\ \rho'<r\leqslant r_e,\ -\pi<\theta\leqslant\pi\right\}\setminus(D_1\cup D_2\cup D_3). \tag{30}$$

Here, note that $\dot{r}>0$ on D_1 from (14), and $\dot{\theta}<0$ on D_2 and D_3 from (15).

Since the characteristics of the velocity field are changed according to (r_0,θ_0) and σ, we consider the convergence in the following four cases: case 1 ($\sigma=0$); case 2 ($\sigma\neq 0$ and $U^*<U'/2$); case 3 ($\sigma\neq 0$ and $U'/2\leqslant U^*<$

$\sqrt{1+\sigma^2}U'/2$); and case 4 ($\sigma \neq 0$ and $\sqrt{1+\sigma^2}U'/2 \leqslant U^* \leqslant U'$). Figure 4 shows the subregions D_1, D_2, D_3, and D_4 for the corresponding cases, and the arrows show the direction of the velocity field on the boundaries of the regions. In case 1, we define the following region D as shown in Figure 5 (a):

$$D = \left\{ (r,\theta) \ : \ \rho' < r \leqslant r_e, \ |\theta| < \frac{\pi}{2} \right\}. \tag{31}$$

For case 2, any r on D_1 satisfies $r < r_c$. A region D for case 2 is defined as follows (see Figure 5 (b)):

$$D = \left\{ (r,\theta) \ : \ \rho' < r < \min\left\{ \rho' + \frac{U^*}{\sigma a}, \ r_c \right\}, \ |\theta| < \frac{\pi}{2} \right\}. \tag{32}$$

For case 3, there exists an r satisfying $r \geqslant r_c$ on D_1, and $r_0 < r_c$. A region D in this case is defined as shown in Figure 5 (c). In case 4, there exists an r satisfying $r \geqslant r_c$ on D_1, and $r_0 \geqslant r_c$. A region D in this case is defined as shown in Figure 5 (d). Now, we show that the trajectory is included in the region D after a certain time.

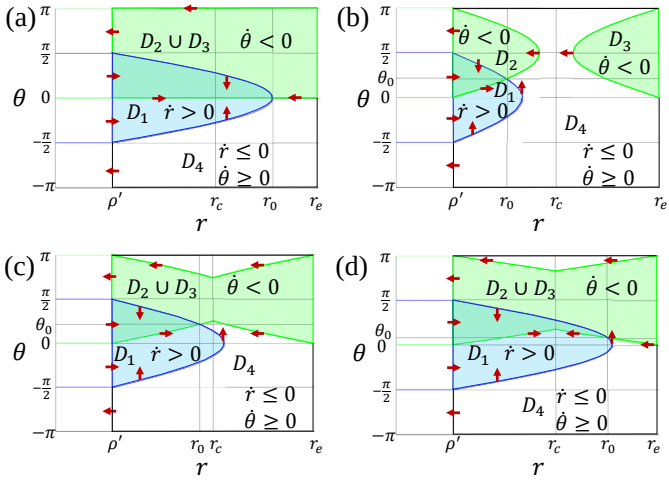

Fig. 4. Velocity fields: (a) Case 1; (b) Case 2; (c) Case 3; (d) Case 4

Lemma, 3. For any initial state $(r(0),\theta(0)) \in (\rho', r_e] \times (-\pi, \pi]$, *there exists* $\tau \geqslant 0$ *such that* $(r(t),\theta(t)) \in D$ *for any* $t \geqslant \tau$.

Proof. For case 1, we divide the whole region into the subregions as shown in Figure 4 (a). Because of the characteristics of the velocity field in

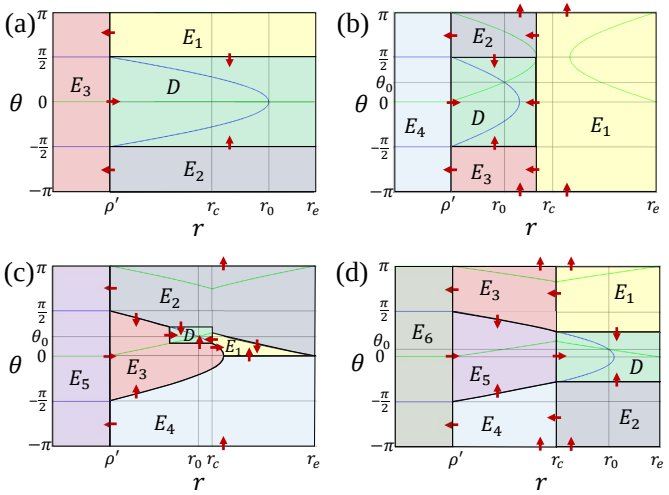

Fig. 5. Divided regions: (a) case 1; (b) case 2; (c) case 3; (d) case 4

case 1, once the trajectory goes inside region D, it stays in D. Thus, we discuss the cases where the initial state is not on D:

1) If (r, θ) is in region E_1 defined in Figure 5 (a); the state goes into D or E_3 defined in Figure 5 (a).

2) If (r, θ) is in the region E_2 defined in Figure 5 (a); the state goes into D or E_3.

3) If (r, θ) is in the region E_3; the state goes into D by Lemma 2.

Thus, in case 1, we found that the state goes into D from any initial state. In other cases, we can show that the state goes into D in the same manner. Therefore, the state goes into D from any initial state in all cases. □

For case 1, $\dot{r}$ and $\dot{\theta}$ in D are C^1 functions of r and θ from (8) and (9). The trajectory is bounded after the state enters D from Lemma 3. Further, the equilibrium is isolated from Lemma 1. Thus, the trajectory behavior for $t \to \infty$ is limited to three cases in Theorem 1.

Since

$$\frac{\partial \dot{r}}{\partial r} + \frac{\partial \dot{\theta}}{\partial \theta} = -a - \frac{U^*}{r} \cos\theta < 0 \tag{33}$$

on D from (8), (9), (14), and (15), there is no periodic orbit by Bendixson's criterion [29], and thus the second case in Theorem 1 is negated. In addition, since there is just one equilibrium on D and there is no trajectory that starts from the equilibrium from Lemma 1, the third case in Theorem 1 is also

negated. Thus, the trajectory that starts from any point on D converges to the equilibrium. The trajectory after a certain time is included in D from Lemma 3, and thus the trajectory from any initial state converges to the equilibrium. For cases 2, 3, and 4, we can show that the trajectory from any initial state converges to the equilibrium in the same manner as in case 1.

4.2. Equilibrium point of bearing angle.

Lemma, 4. (Convergence of bearing angle): Consider the system (16). *For any initial condition* $\phi(t') \in [-\psi, \psi]$, $\phi(t) \to 0$ *as* $t \to \infty$.

Proof. From section 4.1, $\dot{\theta} \to 0$ as $t \to \infty$. If $\dot{\theta}(t) = 0$, solving (16) gives $\phi(t) = \exp(-k(t-t'))\phi(t')$. For arbitrary initial value $\phi(t') \in [-\psi, \psi]$, $\phi(t)$ converges to 0 as $t \to \infty$. Moreover, $\phi(t) \in [-\psi, \psi]$ always holds as shown in [26]. Therefore, from the converging-input and converging-state theorem [30], $\phi(t) \to 0$ as $t \to \infty$. □

The equilibrium state of bearing angle $\phi = 0$ means that the agent is always aiming at its target. Since the relative positions of follower i and its target j converges, the orientation η of follower i converges to the equilibrium state.

4.3. Stability of the whole swarm. Sections 4.1 and 4.2 show that the relative position, bearing angle, and orientation of agent i and its target j converge to the equilibrium if the target j moves at a constant velocity. When the leader moves at a constant velocity, the velocity of follower j, whose target is the leader, converges to that of the leader. Now, let agent k be an agent whose target is agent j, and define r_k, θ_k, and α_j as shown in Figure 6.

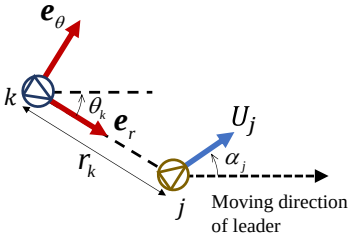

Fig. 6. Definition of r_k, θ_k, and α_j

In this subsection, we hereafter omit the subscript k. The kinematic model of this motion is written as follows:

$$\dot{r} = U_j \cos(\theta + \alpha_j) - u_{kr}, \tag{34}$$

$$\dot{\theta} = \frac{1}{r}\{u_{k\theta} - U_j \sin(\theta + \alpha_j)\}, \tag{35}$$

where U_j is the velocity of agent j, θ is the angle between $\boldsymbol{e}_r$ and the moving direction of the leader, and α_j is the angle between U_j and the moving direction of the leader.

Here, note that kinematic model (34) and (35) become (14) and (15) when $U_j = U^*$. To show the stability of the system (34) and (35), we need to show the boundedness of r and θ. From [26], r is bounded. To show the boundedness of θ, we rewrite (34) and (35) as follows:

$$\dot{r} = U^* \cos\theta - u_{kr} + \mu_r, \tag{36}$$

$$\dot{\theta} = \frac{1}{r}(u_{k\theta} - U^* \sin\theta + \mu_\theta), \tag{37}$$

where $\mu_r = U_j \cos(\theta + \alpha_j) - U^* \cos\theta$, and $\mu_\theta = -U_j \sin(\theta + \alpha_j) + U^* \sin\theta$.

Here, μ_r and μ_θ are bounded because U_j and U^* are bounded. Moreover, since $U_j \to U^*$ and $\alpha_j \to 0$ as $t \to \infty$ from Section 4.1, $\mu_r \to 0$ and $\mu_\theta \to 0$ as $t \to \infty$. That is, for any $\varepsilon > 0$, there exists $T > 0$ such that $|\mu_r| < \varepsilon$ and $|\mu_\theta| < \varepsilon$ hold for $t > T$. This means that we can consider arbitrarily small μ_r and μ_θ (i.e., arbitrarily small $|U_j - U^*|$ and $|\alpha_j|$) after a sufficient period of time.

Here, note that $\dot{\theta}$ is bounded [26], and thus θ is bounded within a sufficiently large finite time. Therefore, we investigate the boundedness of θ after a sufficient period of time.

To show the boundedness of θ after a large enough lapse of time – that is, (34) and (35) with arbitrarily small $|U_j - U^*|$ and $|\alpha_j|$ – we use the same procedures described in Section 4.1. Now, we divide the whole region into the following four subregions:

$$D_1 = \left\{ (r,\theta) \ : \ 0 < r < \rho' + \frac{U_j}{a}\cos(\theta + \alpha_j),\ -\frac{\pi}{2} < \theta + \alpha_j < \frac{\pi}{2} \right\}. \tag{38}$$

$$D_2 = \begin{cases} \left\{ (r,\theta) \ : \ 0 < r < \min\left\{ r_e, \rho' + \frac{U^*}{\sigma a}\sin(\theta + \alpha_j) \right\},\ 0 < \theta + \alpha_j < \pi \right\} \\ \qquad\qquad (0 < \sigma \leqslant 1), \\ \left\{ (r,\theta) \ : \ 0 < r < r_e,\ 0 < \theta + \alpha_j < \pi \right\} \qquad (\sigma = 0), \end{cases} \tag{39}$$

$$D_3 = \begin{cases} \left\{ (r,\theta) \ : \ \max\left\{ 0, r_e - \frac{U^*}{\sigma a}\sin(\theta + \alpha_j) \right\} < r \leqslant r_e,\ 0 < \theta + \alpha_j < \pi \right\} \\ \qquad\qquad (0 < \sigma \leqslant 1), \\ \left\{ (r,\theta) \ : \ 0 < r \leqslant r_e,\ 0 < \theta + \alpha_j < \pi \right\} \qquad (\sigma = 0). \end{cases} \tag{40}$$

Here, note that $\dot{r} > 0$ on D_1 from (34), and $\dot{\theta} < 0$ on D_2 and D_3 from (35), and the remaining part, D_4, is (30).

In addition, we consider the following four cases; case 1 ($\sigma = 0$); case 2 ($\sigma \neq 0$ and $U^* \leqslant U'/2$); case 3 ($\sigma \neq 0$ and $U'/2 < U^* < \sqrt{1+\sigma^2}U'/2$); and case 4 ($\sigma \neq 0$ and $\sqrt{1+\sigma^2}U'/2 \leqslant U^* \leqslant U'$). Figure 7 (a), (b), (c), and (d) show the properties of the velocity fields for cases 1, 2, 3, and 4, respectively.

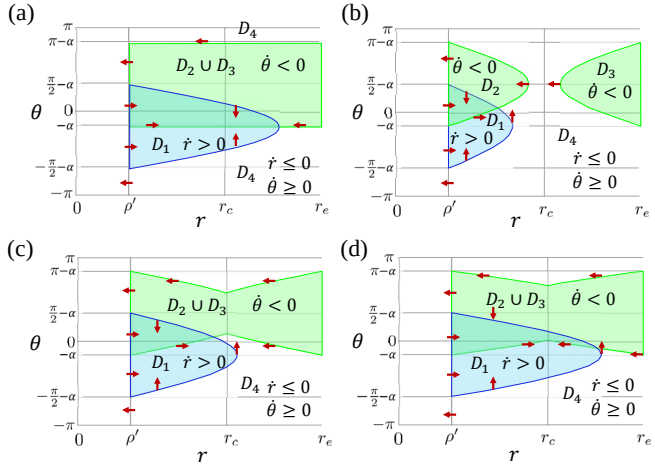

Fig. 7. Properties of the velocity fields

Lemma, 5. (Boundedness of perturbation): In all cases, θ of the kinematic model (34) *and* (35) *with arbitrarily small $|U_j - U^*|$ and $|\alpha_j|$ is bounded.*

Proof. For cases 1, 3, and 4, we found that $D_2 \cap D_3 \neq \emptyset$. Further, from the characteristics of the velocity fields (Fig. 7 (a), (c), and (d)), the state cannot move by stepping over $D_2 \cup D_3$. Thus, θ is bounded. On the other hand, in case 2, we can show that the state goes into D and it stays in D forever, as shown in the proof of Lemma 3, where

$$D = \left\{ (r,\theta) \ : \ \rho' < r < \min\left\{ r_e, \rho' + \frac{U^*}{\sigma a} \right\}, \right. \\ \left. -\frac{\pi}{2} - \alpha_j < \theta < \frac{\pi}{2} - \alpha_j \right\}. \qquad (41)$$

Thus, θ is bounded for case 2. □

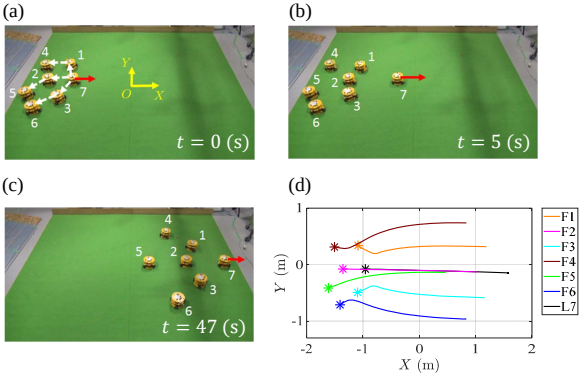

Fig. 8. Experimental environment and trajectories of agents: (a)–(c) Screenshots of experiment; (d) trajectories of all agents

To summarize, the kinematic model (36) and (37) has the following properties: $\mu_r \to 0$ and $\mu_\theta \to 0$ as $t \to \infty$; (36) and (37) become (14) and (15) when $\mu_r = 0$ and $\mu_\theta = 0$; and r and θ are bounded.

Applying the converging-input and converging-state theorem [30], we found that the state (r, θ) of agent k converges to the equilibrium, and its translational velocity converges to that of the leader. Then, since $\dot{\theta} \to 0$, bearing angle ϕ of agent k also converges to the equilibrium point from the Section 4.2. This procedure can be applied to any agent l, whose target is the leader, or agent j, or agent k. Therefore, all agents eventually converge to the equilibrium, and the velocity consensus is achieved. Finally, this section is summarized in the following theorem.

Theorem, 2. (Stability of the whole swarm): If the leader moves at a constant velocity, the control inputs (5)–(9) *and* (11) *realize the following: the shape of the swarm and orientation of all followers converge to the equilibrium state, and the velocity consensus is achieved for all agents.*

5. Experimental Results. We carried out an experiment to confirm the stability of the swarm robots by our control method. We used 7 omnidirectional robots controlled by velocity commands via Bluetooth. Here, the translational velocity and angular velocity of robots could be controlled independently. A motion-capture system measured the positions and orientations of robots. The system was centrally controlled, but the controller for each agent used only local information. Therefore, the controller in this experiment was decentralized. The sampling time was 0.1 (s), and the specifications of follower i are listed in Table 1.

Table 1. Specifications of Followers in the Experiment

Follower i	1	2	3	4	5	6
ρ_i	1.00	0.90	1.00	0.85	0.95	0.80
ρ_i'	0.60	0.55	0.60	0.55	0.55	0.50
ρ_i''	0.40	0.35	0.40	0.40	0.35	0.30
ψ_i	$\pi/4$	$\pi/6$	$\pi/5$	$\pi/4$	$\pi/5$	$\pi/5$
A_i	0.5	0.5	0.5	0.5	0.5	0.5
Ω_i	$2\pi/5$	$\pi/3$	$2\pi/5$	$2\pi/5$	$3\pi/5$	$2\pi/5$
B_i	$\pi/2$	$\pi/2$	$\pi/2$	$\pi/2$	$\pi/2$	$\pi/2$
σ_i	1.0	0.0	-1.0	1.0	0.0	-1.0
V_i	0.19	0.16	0.18	0.19	0.17	0.15
k_i	1.00	1.22	1.12	1.00	1.12	1.12

Table 2. Specifications of Followers in the Numerical Simulation.

i	1	2	3	4	5	6	7	8	9	10
ρ_i	4.1	4.0	4.0	4.8	5.3	4.2	5.9	5.0	6.7	4.0
ρ_i'	1.3	1.3	1.3	1.3	1.3	1.3	1.3	1.3	1.3	1.3
ρ_i''	1.0	1.0	1.0	1.0	1.0	1.0	1.0	1.0	1.0	1.0
ψ_i	$\pi/6$	$\pi/6$	$\pi/6$	$\pi/6$	$\pi/6$	$\pi/6$	$\pi/6$	$\pi/6$	$\pi/6$	$\pi/6$
A_i	0.3	0.4	0.6	0.5	0.5	0.9	0.9	0.7	0.4	0.6
Ω_i	$3\pi/4$	$2\pi/3$	$\pi/2$	$2\pi/3$	$2\pi/3$	$\pi/2$	$2\pi/3$	$3\pi/4$	$2\pi/3$	$2\pi/3$
B_i	π	$3\pi/4$	$\pi/2$	$2\pi/3$	$3\pi/4$	π	$\pi/2$	π	$3\pi/4$	$3\pi/4$
σ_i	0.0	0.0	1.0	1.0	1.0	-1.0	-1.0	-1.0	0.0	1.0
V_i	0.30	0.34	0.36	0.36	0.37	0.47	0.41	0.43	0.34	0.39
k_i	1.37	1.50	1.22	1.41	1.50	1.73	1.22	1.73	1.50	1.50

The leader moved in a straight line at a moving speed first of 0.15 (m/s), then decelerating to 0.045 (m/s) at $t = 5$ (s). This motion makes U' larger for each robot, which resulted in the wider shape of the swarm. Here, note that the purpose of this experiment is not to show that the proposed controller is also applicable when the speed of the leader changes. Figure 8 contains screenshots and shows the trajectories of all agents. In Figure 8 (a), the red arrow shows the leader's moving direction, and the white arrows indicate connectivity, pointing from a follower to a target. Here, the symbol '$*$' shows the initial position of the corresponding robot, and F1, $\cdots$, F6 are the followers, while L7 is the leader. On the other hand, Figure 9 (a), (b), and (c) show the error between each state and its equilibrium point $r - r_0$, $\theta - \theta_0$, and $\phi - \phi_0$, respectively. From these results, the errors converge to zero, and thus the convergence of the state (r, θ, ϕ) is confirmed.

6. Simulation Results. We carried out a numerical simulation to investigate the stability of the swarm robots by our control method for a larger number of robots. In the simulation, we used one leader and 10 followers, and the specifications of follower i are listed in Table 2. In the

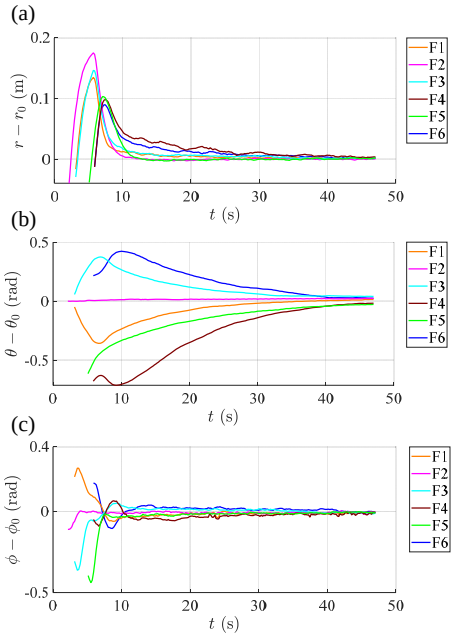

Fig. 9. Experimental results: (a) $r - r_0$. (b) $\theta - \theta_0$. (c) $\phi - \phi_0$

numerical simulation, the leader moved in a straight line, and the leader's initial moving speed was 0.30 (m/s), followed by deceleration to 0.15 (m/s) at $t = 25$ (s), as in the case of the experiment.

Figure 10 shows the simulation results. Figure 10 (a) shows the trajectories of all agents. In this figure, all agents were near the origin at the initial time, then moved in the positive X-axis direction, where F1, $\cdots$, F10 are the followers, while L11 is the leader. On the other hand, Figure 10 (b), (c), and (d) show the error between each state and its equilibrium point $r - r_0$, $\theta - \theta_0$, and $\phi - \phi_0$, respectively. From these results, we found that the errors converge to zero, and thus the convergence of the state (r, θ, ϕ) is confirmed by the numerical simulation.

7. Conclusions. This paper presented a stability analysis of a decentralized navigation method for heterogeneous swarm robots with a limited field of view. Each robot had unique abilities in terms of velocity, acceleration, and sensing region. We proved that the swarm shape and orientation of the followers converged to the equilibrium state when the leader moved at a constant velocity. We also confirmed the stability of an experiment and

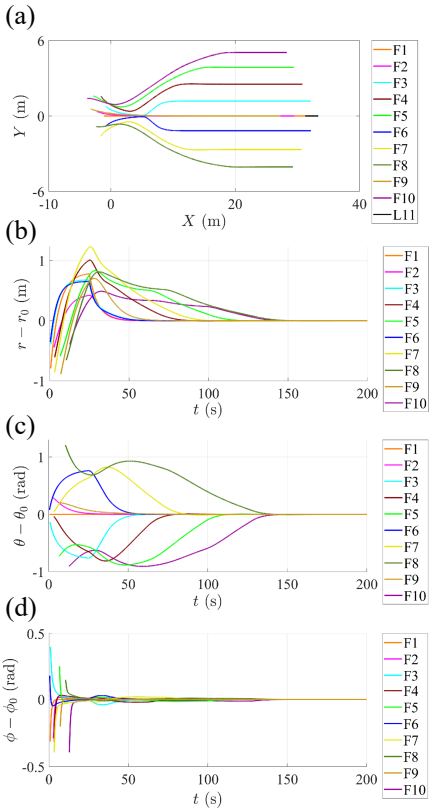

Fig. 10. Simulation results: (a) trajectories of all agents; (b) $r - r_0$; (c) $\theta - \theta_0$; (d) $\phi - \phi_0$

numerical simulation. Future work will be focused on collision avoidance with robots or environmental obstacles by designing the $\boldsymbol{e}_\theta$ component of the control input. We will also investigate line-of-sight (LOS) maintenance between robots, which is important if the robot is equipped with a distance or visual sensor.

References

1. E. Şahin, Swarm Robotics: From Sources of Inspiration to Domains of Application. Swarm Robotics. 2005. pp. 10–20.
2. Brambilla M., Ferrante E., Birattari M., Dorigo M. Swarm robotics: a review from the swarm engineering perspective. *Swarm Intell*. 2013. vol. 7. pp. 1–41.
3. Bayindir L. A review of swarm robotics tasks. *Neurocomputing*. 2016. vol. 172. pp. 292–321.

4. Ge X. et al. A survey on recent advances in distributed sampled-data cooperative control of multi-agent systems. *Neurocomputing*. 2018. vol. 275. pp. 1684–1701.
5. Chung S. et al. Survey on Aerial Swarm Robotics. *IEEE Trans. Robot.*. 2018. vol. 34. pp. 837–855.
6. Nedjah N., Junior L.S. Review of methodologies and tasks in swarm robotics towards standardization. *Swarm and Evolutionary Computation*. 2019. vol. 50. pp. 100565.
7. Kantaros Y., Thanou M., Tzes A. Distributed coverage control for concave areas by a heterogeneous Robot-Swarm with visibility sensing constraints. *Automatica*. 2015. vol. 53. pp. 195–207.
8. Teruel E., Aragues R., López-Nicolás G. A distributed robot swarm control for dynamic region coverage. *Robot. Auton. Syst.*. 2012. vol. 32. pp. 81–95.
9. Durham J.W., Franchi A., Bullo F. Distributed pursuit-evasion without mapping or global localization via local frontiers. *Auton. Robot.*. 2012. vol. 32. pp. 81–95.
10. Garcia-Aunon P., Roldán J., Barrientos A. Monitoring traffic in future cities with aerial swarms: Developing and optimizing a behavior-based surveillance algorithm. *Cognitive Systems Research*. 2019. vol. 54. pp. 273–286.
11. Kim T., Sugie T. Cooperative control for target-capturing task based on a cyclic pursuit strategy. *Automatica*. 2007. vol. 43. pp. 1426–431.
12. Kawakami H., Namerikawa T. Cooperative target-capturing strategy for multivehicle systems with dynamic network topology. Proc. of 2009 American Control Conference. 2009. pp. 635–640.
13. Miyata N., Ota J., Arai T., Asama H. Cooperative transport by multiple mobile robots in unknown static environments associated with real-time task assignment. *IEEE Trans. Robot. Autom.*. 2002. vol. 18. pp. 769–780.
14. Chen J. et al. Occlusion-Based Cooperative Transport with a Swarm of Miniature Mobile Robots. *IEEE Trans. Robot.*. 2015. vol. 31. pp. 307–321.
15. Xu M. et al. Collective Crowd Formation Transform with Mutual Information–Based Runtime Feedback. *Comput. Graph. Forum.*. 2015. vol. 34. pp. 60–73.
16. Kobayashi Y., Endo T., Matsuno F. Distributed formation for robotic swarms considering their crossing motion. *Journal of the Franklin Institute*. 2018. vol. 355. pp. 8698–8722.
17. Dorigo M. et al. Swarmanoid: A Novel Concept for the Study of Heterogeneous Robotic Swarms. *IEEE Robot. Autom. Mag.*. 2013. vol. 20. pp. 60–71.
18. Sabattini L., Secchi C., Chopra N. Decentralized Estimation and Control for Preserving the Strong Connectivity of Directed Graphs. *IEEE Trans. Cybern.*. 2015. vol. 45. pp. 2273–2286.
19. Filotheou A., Nikou A., Dimarogonas D.V. Robust decentralised navigation of multi-agent systems with collision avoidance and connectivity maintenance using model predictive controllers. *Int. J. Control*. 2020. vol. 93. no. 6. pp. 1470–1484.
20. Yoo S.J., Park B.S. Connectivity preservation and collision avoidance in networked nonholonomic multi-robot formation systems: Unified error transformation strategy. *Automatica*. 2019. vol. 103. pp. 274–281.
21. Yoshimoto M., Endo T., Maeda R., Matsuno F. Decentralized navigation method for a robotic swarm with nonhomogeneous abilities. *Auton. Robots*. 2018. vol. 42. pp. 1583–1599.
22. Panagou D., Kumar V. Cooperative Visibility Maintenance for Leader–Follower Formations in Obstacle Environments. *IEEE Trans. Robot.*. 2014. vol. 30. pp. 831–844.
23. Delimpaltadakis I.M., Bechlioulis C.P., Kyriakopoulos K.J. Decentralized Platooning With Obstacle Avoidance for Car-Like Vehicles With Limited Sensing. *IEEE Robot. Autom. Lett.*. 2018. vol. 3. pp. 835–840.
24. Liu X., Ge S.S., Goh C. Vision-Based Leader–Follower Formation Control of Multiagents With Visibility Constraints. *IEEE Trans. Control Syst. Technol.*. 2019. vol. 27. pp. 1326–1333.

25. Poonawala H.A., Spong M.W. Cooperative visibility maintenance in SE(3) for multirobot-networks with limited field-of-view sensors. *Control Theory Technol.*. 2017. vol. 15. pp. 246–257.
26. Maeda R., Endo T. Matsuno F. Decentralized Navigation for Heterogeneous Swarm Robots With Limited Field of View. *IEEE Robotics and Automation Letters*. 2017. vol. 2. pp. 904–911.
27. Endo T., Maeda R. Matsuno F. Stability Analysis for Heterogeneous Swarm Robots with Limited Field of View. Proc. of 2019 Developments in eSystems Engineering (DeSE). 2019. pp. 27–32.
28. Alligood K.T., Sauer T.D., Yorke J.A. Chaos: An introduction to dynamical systems. Springer. 1996. 358 p.
29. Li Y., Muldowney J.S. On Bendixson's criterion. *J. Differ. Equations*. 1993. vol. 106. pp. 27–39.
30. Sontag E.D. A remark on the converging-input converging state property. *IEEE Trans. Automat. Contr.*. 2003. vol. 48. pp. 313–314.

Takahiro Endo — Ph.D., Associate Professor, Kyoto University. Research interests: robotics, haptics, and control of infinite dimensional system. The number of publications — 43. endo@me.kyoto-u.ac.jp; C3, Kyodai Katsura, Nishikyo-ku, 615-8540, Kyoto, Japan; office phone: 81-75-383-3595; fax: +81-75-383-3595.

Ryuma Maeda — Master's Student, Department of Mechanical Engineering and Science, Kyoto University. Research interests: control of multi-agent system. The number of publications — 3. ray501.itsme182@gmail.com; C3, Kyodai Katsura, Nishikyo-ku, 615-8540, Kyoto, Japan; office phone: +81-75-383-3595; fax: +81-75-383-3595.

Fumitoshi Matsuno — Ph.D., Professor, Department of Mechanical Engineering and Science, Kyoto University. Research interests: robotics, swarm intelligence, control of distributed parameter system and nonlinear system, rescue support system in disaster. The number of publications — 181. matsuno@me.kyoto-u.ac.jp; C3, Kyodai Katsura, Nishikyo-ku, 615-8540, Kyoto, Japan; office phone: +81-75-383-3595; fax: +81-75-383-3595.

Acknowledgements. This work was supported in part by JST SICORP Grant Number JP-MJSC18E4, Japan.

УДК 004.9 **DOI** 10.15622/ia.2020.19.5.2

Т. Эндо, Р. Маэда, Ф. Мацуно

АНАЛИЗ УСТОЙЧИВОСТИ РОЯ ГЕТЕРОГЕННЫХ РОБОТОВ С ОГРАНИЧЕННЫМ ПОЛЕМ ЗРЕНИЯ

Эндо Т., Маэда Р., Мацуно Ф. **Анализ устойчивости роя гетерогенных роботов с ограниченным полем зрения.**

Аннотация. Представлен анализ устойчивости роя гетерогенных роботов, где каждый робот имеет разный уровень чувствительности сенсоров и различные физические ограничения, включая максимальную скорость движения и ускорения. Каждый робот обладает уникальной областью восприятия в условиях ограниченного поля зрения. Изначально предлагался децентрализованный метод навигации для роя гетерогенных роботов, состоящего из ведущего робота и многочисленных ведомых роботов. С децентрализованным методом навигации ведущий робот может направлять ведомых, поддерживая соединение и учитывая физические ограничения, уникальные для каждого робота. Данное исследование сосредоточено на анализе устойчивости равновесия такого роя ргетерогенных роботов. С математической точки зрения доказывается, что когда ведущий робот двигается с постоянной скоростью, форма и направление всех остальных ведомых роботов в конечном счете стремятся к равновесию. Чтобы продемонстрировать совпадение этого состояния равновесия, сперва необходимо доказать, что оно существует. Проводятся эксперименты и численные моделирования, чтобы подтвердить наличие стабильности, то есть достижение роем роботов состояния равновесия.

Ключевые слова: устойчивость, рой роботов, навигация, децентрализованный контроллер

Эндо Такахиро — Ph.D., доцент, Киотский университет. Область научных интересов: робототехника, тактильные ощущения и управление бесконечномерными системами. Число научных публикаций — 43. endo@me.kyoto-u.ac.jp; Кёдай Катсура, Нисикё-ку, С3, 615-8540, Киото, Япония; р.т.: 81-75-383-3595; факс: +81-75-383-3595.

Маэда Рёма — студент магистратуры, кафедра машиностроения и науки, Киотский университет. Область научных интересов: управление мультиагентной системой. Число научных публикаций — 3. ray501.itsme182@gmail.com; Кёдай Катсура, Нисикё-ку, С3, 615-8540, Киото, Япония; р.т.: +81-75-383-3595; факс: +81-75-383-3595.

Мацуно Фумитоси — Ph.D., профессор, кафедра машиностроения и науки, Киотский университет. Область научных интересов: робототехника, разведка роя, управление системой распределенных параметров и нелинейной системой, система поддержки спасения при бедствиях. Число научных публикаций — 181. matsuno@me.kyoto-u.ac.jp; Кёдай Катсура, Нисикё-ку, С3, 615-8540, Киото, Япония; р.т.: +81-75-383-3595; факс: +81-75-383-3595.

Поддержка исследований. Работа выполнена при частичной финансовой поддержке Японского агентсва науки и технологий "Программа стратегических международных совместных исследований" (номер гранта JPMJSC18E4).

Литература

1. *Şahin E.* Swarm Robotics: From Sources of Inspiration to Domains of Application // Swarm Robotics. 2005. pp. 10–20.
2. *Brambilla M., Ferrante E., Birattari M., Dorigo M.* Swarm robotics: a review from the swarm engineering perspective // Swarm Intell. 2013. vol. 7. pp. 1–41.
3. *Bayindir L.* A review of swarm robotics tasks // Neurocomputing. 2016. vol. 172. pp. 292–321.
4. *Ge X. et al.* A survey on recent advances in distributed sampled-data cooperative control of multi-agent systems // Neurocomputing. 2018. vol. 275. pp. 1684–1701
5. *Chung S. et al.* Survey on Aerial Swarm Robotics // IEEE Trans. Robot. 2018. vol. 34. pp. 837–855.
6. *Nedjah N., Junior L.S.* Review of methodologies and tasks in swarm robotics towards standardization // Swarm and Evolutionary Computation. 2019. vol. 50. pp. 100565.
7. *Kantaros Y., Thanou M., Tzes A.* Distributed coverage control for concave areas by a heterogeneous Robot-Swarm with visibility sensing constraints // Automatica. 2015. vol. 53. pp. 195–207.
8. *Teruel E., Aragues R., López-Nicolás G.* A distributed robot swarm control for dynamic region coverage // Robot. Auton. Syst. 2019. vol. 119. pp. 51–63.
9. *Durham J.W., Franchi A., Bullo F.* Distributed pursuit-evasion without mapping or global localization via local frontiers // Auton. Robot. 2012. vol. 32. pp. 81–95.
10. *Garcia-Aunon P., Roldán J., Barrientos A.* Monitoring traffic in future cities with aerial swarms: Developing and optimizing a behavior-based surveillance algorithm // Cognitive Systems Research. 2019. vol. 54. pp. 273–286.
11. *Kim T., Sugie T.* Cooperative control for target-capturing task based on a cyclic pursuit strategy // Automatica. 2007. vol. 43. pp. 1426–431.
12. *Kawakami H., Namerikawa T.* Cooperative target-capturing strategy for multivehicle systems with dynamic network topology // Proc. of 2009 American Control Conference. 2009. pp. 635–640.
13. *Miyata N., Ota J., Arai T., Asama H.* Cooperative transport by multiple mobile robots in unknown static environments associated with real-time task assignment // IEEE Trans. Robot. Autom. 2002. vol. 18. pp. 769–780.
14. *Chen J. et al.* Occlusion-Based Cooperative Transport with a Swarm of Miniature Mobile Robots // IEEE Trans. Robot. 2015. vol. 31. pp. 307–321.
15. *Xu M. et al.* Collective Crowd Formation Transform with Mutual Information–Based Runtime Feedback // Comput. Graph. Forum. 2015. vol. 34. pp. 60–73.
16. *Kobayashi Y., Endo T., Matsuno F.* Distributed formation for robotic swarms considering their crossing motion // Journal of the Franklin Institute. 2018. vol. 355. pp. 8698–8722.
17. *Dorigo M. et al.* Swarmanoid: A Novel Concept for the Study of Heterogeneous Robotic Swarms // IEEE Robot. Autom. Mag. 2013. vol. 20. pp. 60–71.
18. *Sabattini L., Secchi C., Chopra N.* Decentralized Estimation and Control for Preserving the Strong Connectivity of Directed Graphs // IEEE Trans. Cybern. 2015. vol. 45. pp. 2273–2286.
19. *Filotheou A., Nikou A., Dimarogonas D.V.* Robust decentralised navigation of multi-agent systems with collision avoidance and connectivity maintenance using model predictive controllers // Int. J. Control. 2020. vol. 93. no. 6. pp. 1470–1484.
20. *Yoo S.J., Park B.S.* Connectivity preservation and collision avoidance in networked nonholonomic multi-robot formation systems: Unified error transformation strategy // Automatica. 2019. vol. 103. pp. 274–281.

21. *Yoshimoto M., Endo T., Maeda R., Matsuno F.* Decentralized navigation method for a robotic swarm with nonhomogeneous abilities // Auton. Robots. 2018. vol. 42. pp. 1583–1599.
22. *Panagou D., Kumar V.* Cooperative Visibility Maintenance for Leader–Follower Formations in Obstacle Environments // IEEE Trans. Robot. 2014. vol. 30. pp. 831–844.
23. *Delimpaltadakis I.M., Bechlioulis C.P., Kyriakopoulos K.J.* Decentralized Platooning With Obstacle Avoidance for Car-Like Vehicles With Limited Sensing // IEEE Robot. Autom. Lett. 2018. vol. 3. pp. 835–840.
24. *Liu X., Ge S.S., Goh C.* Vision-Based Leader–Follower Formation Control of Multiagents With Visibility Constraints // IEEE Trans. Control Syst. Technol. 2019. vol. 27. pp. 1326–1333.
25. *Poonawala H.A., Spong M.W.* Cooperative visibility maintenance in SE(3) for multirobot-networks with limited field-of-view sensors // Control Theory Technol. 2017. vol. 15. pp. 246–257.
26. *Maeda R., Endo T. Matsuno F.* Decentralized Navigation for Heterogeneous Swarm Robots With Limited Field of View // IEEE Robotics and Automation Letters. 2017. vol. 2. pp. 904–911.
27. *Endo T., Maeda R. Matsuno F.* Stability Analysis for Heterogeneous Swarm Robots with Limited Field of View // Proc. of 2019 Developments in eSystems Engineering (DeSE). 2019. pp. 27–32.
28. *Alligood K.T., Sauer T.D., Yorke J.A.* Chaos: An introduction to dynamical systems // Springer. 1996. 358 p.
29. *Li Y., Muldowney J.S.* On Bendixson's criterion // J. Differ. Equations. 1993. vol. 106. pp. 27–39.
30. *Sontag E.D.* A remark on the converging-input converging state property // IEEE Trans. Automat. Contr. 2003. vol. 48. pp. 313–314.